




Article

Reduced-Order Model of a Time-Trial Cyclist Helmet for Aerodynamic Optimization Through Mesh Morphing and Enhanced with Real-Time Interactive Visualization

E. Di Meo , A. Lopez, C. Groth, M. E. Biancolini * and P. P. Valentini 

Department of Enterprise Engineering, University of Rome "Tor Vergata", Via del Politecnico 1, 00133 Rome, Italy; emanuele.di.meo@uniroma2.it (E.D.M.); lopez@ing.uniroma2.it (A.L.); corrado.groth@uniroma2.it (C.G.); valentini@ing.uniroma2.it (P.P.V.)

* Correspondence: biancolini@ing.uniroma2.it

Abstract: Aerodynamics is a key factor in time-trial cycling. Over the years, various aspects have been investigated, including positioning, clothing, bicycle design, and helmet shape. The present study focuses on the development of a methodology for the aerodynamic optimization of a time-trial helmet through the implementation of a reduced-order model, alongside advanced simulation techniques, such as computational fluid dynamics, radial basis functions, mesh morphing, and response surface methodology. The implementation of a reduced-order model enhances the understanding of aerodynamic interactions compared to traditional optimization workflows reported in sports-related research, facilitating the identification of an optimal helmet shape during the design phase. The study offers practical insights for refining helmet design. Starting with a baseline teardrop profile, several morphing configurations are systematically tested, resulting in a 10% reduction in the drag force acting on the helmet. The reduced-order model also facilitates the analysis of turbulent flow patterns on the cyclist's body, providing a detailed understanding of aerodynamic interactions. By leveraging reduced-order models and advanced simulation techniques, this study contributes to ongoing efforts to reduce the aerodynamic resistance of time-trial helmets, ultimately supporting the goal of improved athlete performance.

Keywords: aerodynamics; reduced-order model; mesh morphing; optimization; cycling



Citation: Di Meo, E.; Lopez, A.; Groth, C.; Biancolini, M.E.; Valentini, P.P.

Reduced-Order Model of a Time-Trial Cyclist Helmet for Aerodynamic Optimization Through Mesh Morphing and Enhanced with Real-Time Interactive Visualization.

Fluids **2024**, *9*, 300. <https://doi.org/10.3390/fluids9120300>

Academic Editors: Mesbah Uddin and Mahmoud Mamou

Received: 22 October 2024

Revised: 11 December 2024

Accepted: 14 December 2024

Published: 17 December 2024



Copyright: © 2024 by the authors. Licensee MDPI, Basel, Switzerland. This article is an open access article distributed under the terms and conditions of the Creative Commons Attribution (CC BY) license (<https://creativecommons.org/licenses/by/4.0/>).

1. Introduction

In recent years, aerodynamics has gained increasing importance across various sports. Initially confined to motorsports, such as Formula and GT racing, aerodynamics has now found application across a diverse range of athletic disciplines. From speed-focused sports like cycling, ski jumping, sprinting, and skating to ball sports, such as football, tennis, and golf, extensive research has been conducted on integrating aerodynamic principles into equipment, clothing, and even ball designs [1]. In this context, cycling has long prioritized aerodynamics, with a notable increase in its significance in recent years, particularly within the time-trial discipline.

A time trial in cycling is a race format in which participants, individually or as part of a team, race against the clock rather than directly against each other. In such races, achieving optimal aerodynamics is critical to minimize drag, which directly affects performance by reducing the braking effect. Aerodynamics plays a crucial role in cycling, as races are often decided by seconds or even fractions of a second. There are numerous examples of this importance [2], one of the most notable being Greg LeMond's victory in the 1989 Tour de France. LeMond overcame a 50 s gap to the overall leader, Laurent Fignon, in the final stage, an individual time trial, to win the Tour by just 8 s. This remarkable comeback was aided by LeMond's advanced equipment, which included airfoil-shaped tubing, an aerodynamic helmet, and a disc rear wheel, while Fignon rode a standard bike without a helmet.

Previous research [3,4] indicates that aerodynamic drag contributes up to 90% of braking at speeds above 40 km/h, with rolling resistance responsible for the remaining portion. Optimal cyclist positioning plays a crucial role in minimizing aerodynamic drag, which accounts for 60–82% of the total drag [5,6], while helmet choice can influence drag by approximately 2–8% [7,8]. These topics have been extensively studied by cycling teams and specialized research groups. Despite the limitations imposed by the Union Cycliste Internationale's regulations, many innovative solutions have been proposed. Notable examples include the Visma Lease-a-Bike time-trial helmet presented in March 2024 [9] and the use of chest fairings [10].

In this context, the study focuses on creating a methodology using a reduced-order model (ROM) for the aerodynamic optimization of a time-trial helmet. Compared to a standard optimization workflow using response surface optimization (RSM), implementing a ROM provides a more comprehensive understanding of the aerodynamic interactions, describing complete fields such as pressure and turbulence intensity. The ROM, through the extraction of dominant system modes, allows a real-time evaluation of the model amid the flow complexity and vast amount of data analyzed in full-order simulations, as highlighted in several research studies with reference to linear, non-linear [11,12], and dynamic systems [13], with particular application in the aeronautical field [14–16]. The use of a ROM allows a quick and accurate assessment of the dominant features of the system, providing in-depth support during the design phase and giving direction to the design choices to be made. The ROM can be enhanced with experimental data from the cyclist and helmet. For instance, pressure sensors can be installed on the cyclist's body and helmet to measure pressure values at various points. These data can then be integrated with simulation data to create an even more accurate ROM. Although many research studies on aerodynamic optimization in sports engineering have been conducted, to the authors' knowledge, the use of ROMs in these areas is not yet widely adopted, particularly in cycling.

The aim of the present study is to deploy an accurate ROM for time-trial helmets' interactive optimization. The main novelty of this contribution lies in extending traditional optimization procedures used in sports aerodynamics through the integration of a ROM, enabling a more detailed understanding of flow interactions and supporting the design phase with real-time assessment of aerodynamic fields. The material presented is organized as follows: Section 1, this introduction, presents the state of the art regarding advanced CFD adoption in time-trial cycling; Section 2, the mathematical background and the implementation details of the proposed approach are given; Section 3, the case study investigated is detailed; the results are presented and discussed in the Section 4 and then completed by Section 5.

2. Methodology

The implementation of a reduced-order model in a computational analysis involves several steps across the different simulation phases. With a particular reference to model order reduction applied to fluid dynamics [17–20], the proposed methodology is developed as illustrated in Figure 1. First, a baseline model is implemented, and simulations are performed. The parameters of interest, which may be geometrical or physical, are then identified. Physical parameters are related to quantities describing the physics of the problem, such as force, inlet velocity, or applied pressure, while geometrical parameters are connected to the shape of the simulated elements and can be handled through parametrization of the computer-aided design (CAD) model or by parametrizing the mesh using mesh morphing techniques. The parameterization of the computational model allows for the implementation of a design of experiments (DoE), resulting in the creation of a series of design points. Each design point is simulated to generate a set of full-scale (or full-order) model simulations. The results of these simulations are stored and used to build the ROM. The ROM is generated using simulation results through a combination of modal bases. ROM exploration provides detailed information regarding the evaluated quantities

across the parameter range, with valuable insights for design optimization. In parallel, response surface methodology (RSM) [21] is employed to develop a single-value optimization framework. RSM uses statistical techniques [22] to create a functional relationship between the input parameters and the output ones, enabling single-value optimization and multi-objective optimization [23]. While RSM focuses on finding the optimal set of parameters, such as minimum drag coefficient, ROM offers a comprehensive overview of the system’s behavior across the entire range of input parameters. It is worth noting that the approach used for global output exploration with RSM and ROM exploration in the reduced space requires interpolation for both methods to obtain the outputs (such as a global parameter like drag or a reduced coordinate of a ROM) as a function of the inputs.

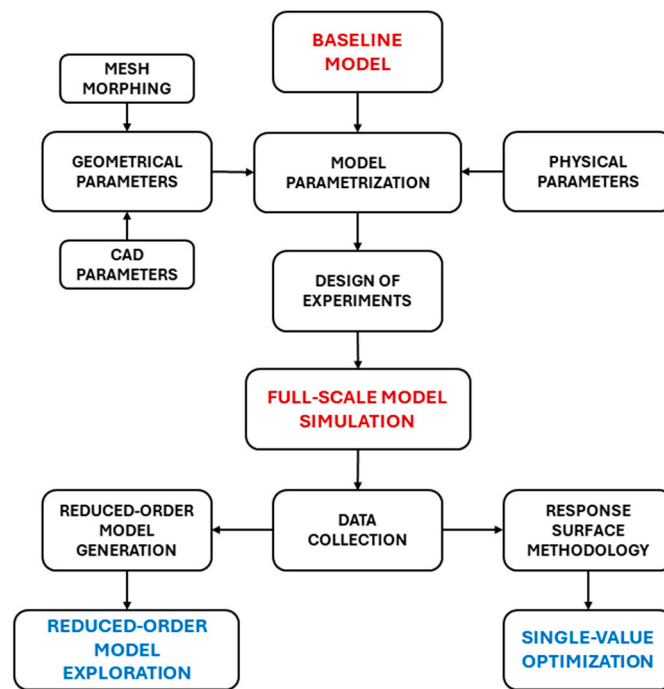


Figure 1. Workflow for ROM and response surface generation.

2.1. Model Order Reduction

Model order reduction (MOR) is a mathematical technique that approximates complex high-dimensional systems to reduce the number of degrees of freedom (DoFs) while preserving essential dynamics. Over the years, several MOR methods have been developed to improve computational efficiency, such as the center manifold, Lyapunov–Schmidt (L-S), Galerkin, principal orthogonal decomposition (POD) methods [19,24,25], and principal component analysis (PCA) [26].

The POD method is a projection-based order reduction method widely used to obtain reduced-order models (ROMs) for dynamic analysis and for parametric design of complex systems. POD identifies the system’s behavior by transforming the original variables (such as pressure, temperature, or stress) into a set of orthogonal modes. This result is obtained by running a series of simulations of the full-order model and collecting the results of each simulation in datasets called snapshots. The creation of a ROM using POD is based on a series of sequential steps. Given a system described by a high-dimensional state vector $\mathbf{x} \in \mathbb{R}^m$ (where m is the number of spatial points or degrees of freedom), snapshots of the full-order model solutions at different parameter configurations are evaluated. Each snapshot differs from the baseline because it is obtained with different physical input parameters, different geometrical input parameters, or both; however, to adopt this method, the snapshot must be defined consistently with respect to the baseline, i.e., adopting the same order and the same number of spatial points or degrees of freedom m . After collecting

the snapshots, a snapshot matrix \mathbf{A} is constructed, with columns corresponding to the number of snapshots, and singular value decomposition (SVD) is applied to decompose it into the product of three matrices [27]:

$$\mathbf{A} = \mathbf{U}\mathbf{\Sigma}\mathbf{V}^T \tag{1}$$

where

- $\mathbf{A} \in \mathbb{R}^{m \times n}$ is the snapshot matrix, where m is the number of spatial points or degrees of freedom of the system, and n is the number of snapshots. Each column of the matrix \mathbf{A} represents a snapshot of the system state at a given parameter value.
- $\mathbf{U} \in \mathbb{R}^{m \times m}$ is an orthonormal matrix, whose columns are left singular vectors containing the dominant spatial modes.
- $\mathbf{\Sigma} \in \mathbb{R}^{m \times n}$ is a diagonal matrix containing singular values ordered in a descending order of magnitude. Larger singular values indicate more significant modes.
- $\mathbf{V}^T \in \mathbb{R}^{n \times n}$ is an orthonormal matrix. The columns of \mathbf{V} are right singular vectors containing the parameter coefficients associated with each snapshot.

Decomposing the snapshot matrix enables the creation of its reduced form, in which the most significant modes are included. If r modes are selected, the reduced matrix \mathbf{A}_r can be written as

$$\mathbf{A}_r = \mathbf{U}_r\mathbf{\Sigma}_r\mathbf{V}_r^T \tag{2}$$

where $\mathbf{A}_r \in \mathbb{R}^{m \times n}$, $\mathbf{U}_r \in \mathbb{R}^{m \times r}$, $\mathbf{\Sigma}_r \in \mathbb{R}^{r \times r}$, $\mathbf{V}_r^T \in \mathbb{R}^{r \times n}$.

The dimension of \mathbf{A}_r remains $m \times n$, as it still represents the m spatial points or degrees of freedom and n snapshots, but its rank is reduced from $\min(m, n)$ to r , preserving the most important features of the original data. The POD-reduced system representation, given by a state vector $\mathbf{y} \in \mathbb{R}^r$, can now be obtained by reducing the full-order model \mathbf{x} by using the reduced spatial modes of matrix \mathbf{U}_r in the following form:

$$\mathbf{y} = \mathbf{U}_r^T\mathbf{x} \tag{3}$$

The state of the full-order model from the reduced-order model can be obtained as

$$\mathbf{x} \approx \mathbf{U}_r\mathbf{y} \tag{4}$$

where the closer the model approximates the original state, the more the selected modes r capture the dominant features of the system.

The key characteristic of the POD method is that reduced modes are obtained by numerical or experimental data snapshots, and it can be fruitfully combined with parametric CAE models ready to create as many snapshots as required to properly train the ROM. The described approach leads to the creation of a ROM that preserves essential system characteristics and high accuracy of the model while significantly reducing the dimensionality of the system representation, with significant advantages in terms of computational time. It is important to note that while ROM evaluation can provide results in very short times (up to real time, with frame rates fast enough for interaction in VR), ROM construction requires a series of full simulations or experimental data collection.

2.2. RBF Mesh Morphing

Mesh morphing is a computational technique widely used in computer graphics, computational fluid dynamics, and finite element analysis [28,29]. It enables efficient adjustments to computational grids or meshes to account for shape variations in the underlying geometry, avoiding the need to regenerate meshes from scratch. Mesh morphing uses parametric displacements to deform the original mesh rather than generating a new mesh from scratch. Compared to traditional workflows, where shape parameters are defined in CAD geometries, mesh morphing offers two major advantages: it preserves mesh quality and significantly reduces computational time, particularly in shape optimization

workflows like the design of experiments. Mesh morphing aims to maintain mesh quality and topology while adapting to variations in the shape or configurations of the simulated object. The preservation of mesh topology is especially critical for developing reduced-order models (ROMs), as it ensures consistency in node definitions across configurations. This technique has been successfully applied in diverse fields, including marine CFD optimization [30], motorsport aerodynamics [31], and biomedical modeling [32].

In this study, mesh morphing is implemented using radial basis functions (RBFs). RBFs are a mathematical tool used to interpolate a scalar function defined in discrete points (called *source points*) to a full domain space [29]. The interpolation function $s(\mathbf{x})$ consists of a radial basis and a polynomial term and is defined as

$$s(\mathbf{x}) = \sum_{i=1}^N \gamma_i \phi(\mathbf{x} - \mathbf{x}_{si}) + h(\mathbf{x}) \tag{5}$$

where N is the number of source points; γ_i are the function weights; $\phi(\|\mathbf{x} - \mathbf{x}_{si}\|)$ is the radial function; \mathbf{x} is the generic point position; \mathbf{x}_{si} is the source point position; $h(\mathbf{x})$ is a polynomial term with a degree dependent on the chosen radial function. In the case of a three-dimensional deformation field, as in space morphing, each displacement component is interpolated individually:

$$\begin{cases} s_x(\mathbf{x}) = \sum_{i=1}^N \gamma_i^x \phi(\mathbf{x} - \mathbf{x}_{si}) + \beta_1^x + \beta_2^x x + \beta_3^x y + \beta_4^x z \\ s_y(\mathbf{x}) = \sum_{i=1}^N \gamma_i^y \phi(\mathbf{x} - \mathbf{x}_{si}) + \beta_1^y + \beta_2^y x + \beta_3^y y + \beta_4^y z \\ s_z(\mathbf{x}) = \sum_{i=1}^N \gamma_i^z \phi(\mathbf{x} - \mathbf{x}_{si}) + \beta_1^z + \beta_2^z x + \beta_3^z y + \beta_4^z z \end{cases} \tag{6}$$

2.3. Design of Experiments and Response Surface Methodology

Design of experiments (DoE) is a statistical approach used to plan experiments and analyze the correlation between the input and output variables of a system. The goal of this methodology is to maximize the gain of information while minimizing the number of experiments required, thus optimizing the use of resources. In simulations, DoE helps identify the most influential factors, their interactions, and their effects on outputs [22,33]. DoE methods rely on the sampling strategies, i.e., the way design variations are defined upfront, and response surface interpolation, i.e., the way the sampled data are retrieved on new-and-not-seen design configurations. The traditional sampling methods include full factorial (FF), central composite design (CCD), and Latin hypercube sampling (LHS).

Response surface methodology (RSM) is an extension of DoE that focuses on modeling output responses determined by a set of input parameters. It involves the use of various mathematical techniques to model a response surface that approximates the relationship between the singular values of the inputs and outputs to create a continuous response over the design space. The main methods used to implement response surfaces are genetic aggregation [34,35], standard response surface with full second-order polynomials [36], kriging [37], non-parametric regression [38], sparse grid [39], and radial basis functions [23].

In this study, genetic aggregation (GA) is used to integrate response surfaces to obtain the genetic aggregation response surface (GARS) method. The GARS method uses genetic algorithms to determine an optimal combination of multiple response surfaces, ensuring that the aggregated model captures the essential characteristics of the provided data. Mathematically, the algorithm can be expressed as follows:

$$G(\mathbf{x}) = \sum_{i=1}^n \omega_i R_i(\mathbf{x}) \tag{7}$$

where $G(\mathbf{x})$ is the aggregated response surface; $R_i(\mathbf{x})$ are the individual response surfaces; and ω_i are the optimized weights. The weight values are evaluated by integrating a

multi-objective genetic algorithm (MOGA) to meet the requirements of the optimization objective.

2.4. Computational Fluid Dynamics

Computational fluid dynamics (CFD) enables the prediction of fluid flow, heat transfer, mass transfer, chemical reactions, and related phenomena by solving mathematical equations that govern these processes through numerical simulations [40]. Most CFD solvers use the finite volume method and implement turbulence models to represent eddies with a wide range of lengths and time scales: Reynolds-averaged Navier–Stokes (RANS) models, large eddy simulation (LES), and direct numerical simulation (DNS). RANS models are widely used in industry [41], as they offer a good balance between computational efficiency and the ability to handle complex turbulent flows. Various RANS turbulence models exist, ranging from simpler one-equation models to complex two-equation models like the k - ϵ and k - ω models [42]. In this study, a 3D steady-state RANS approach is used with a standard K - ϵ turbulence model. The approach builds on previous studies of bicycle aerodynamics [43], highlighting the importance of detailed turbulence modeling, as turbulence can influence drag resistance by up to 20% [44]. CFD simulations, even under the RANS simplifications, are numerically intensive and require high-performance computing to solve the flow in a reasonable time. The computational domains could comprise millions of cells, and a large amount of memory is required to store the data. Reduced-order models can be effectively trained using a reasonable amount of data computed by full-order models as input, which in this study are the CFD simulations.

3. Case Study

The case study aims to optimize the aerodynamics of a cyclist's time-trial helmet under conditions typical of a road individual time-trial (ITT) stage, with the cyclist traveling at a speed of 54 km/h (15 m/s). This comprehensive study involves several steps to achieve the optimal helmet design. First, the cyclist, bicycle, and helmet geometries are modeled as detailed in the following sections. The cyclist's positioning is also accurately implemented to reflect an ITT stage scenario. Next, a computational fluid dynamics mesh is created, and an initial analysis is performed on this baseline case to establish a reference point for subsequent evaluations. Following this, shape parameters are defined on the helmet geometry to guide the optimization process. Mesh morphing techniques are then applied to the initial mesh, enabling adjustments in the geometry based on these defined parameters. To explore the variable space and understand the impact of different helmet shapes, a design of experiments approach is employed. This method facilitates the systematic variation of shape parameters and the execution of corresponding CFD analyses. Subsequently, a response surface methodology is utilized to analyze the results from the DoE and identify the optimal helmet shape for drag minimization. This approach enables the visualization of the relationship between helmet shape parameters and aerodynamic performance. Finally, the deployment of a reduced-order model, combined with mesh morphing, allows real-time visualization of the aerodynamic and turbulence fields across the parameters' range. This integration enhances the understanding of the system by enabling a detailed analysis of flow behavior, illustrating the distribution and interaction of critical fields across both the helmet and the cyclist's body. As a result, this approach significantly improves the design process and performance evaluation, leading to more informed aerodynamic optimizations. This case study was implemented using a combination of open-source and commercial software, as described in the following sections. The proposed workflow can be adapted to other software platforms or solvers, including open-source alternatives.

3.1. Cyclist Modeling and Positioning

The first part of the study focuses on the modeling and positioning of the cyclist on the bicycle. A human body model was imported from the DINED anthropometric database of TU Delft [45] to create the geometric model of the cyclist. This database offers a compre-

hensive dataset derived from scanning a diverse population, providing detailed physical characteristics. Several studies and research projects have been conducted to classify human body models. Among these, the CAESAR project anthropometric database [46,47] was selected to provide the foundational anthropometric data for this analysis. In developing the model, a wide range of parameters can be configured. Specifically, an adult male with a height of 180 cm and a weight of 72 kg was chosen, with other body dimension parameters set at the 50th percentile, resulting in the mannequin model illustrated in Figure 2.

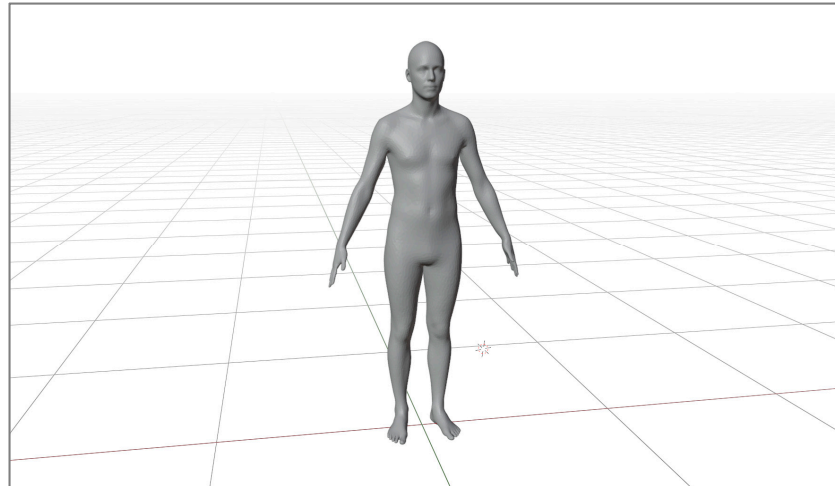


Figure 2. Human body model at the 50th percentile with a height of 1.80 m and a weight of 72 kg.

The model was articulated into a cycling posture using Blender[®] 4.2 software, utilizing its rigging capabilities. Rigging in computer graphics refers to the process of creating a digital skeleton for a 3D model, allowing it to be animated [48,49]. This skeleton is composed of “bones” or control structures that enable the model to move in realistic ways, as already demonstrated in studies across diverse scientific fields [50,51]. The process starts with the import of the STL file providing the baseline geometry of the standing cyclist. The skeletal structure, or armature, is created within Blender through the *Rigify* add-on, selecting a basic human rig template to approximate the cyclist’s anatomy. The articulation rig, consisting of 58 bones, is then accurately aligned with the standing cyclist, and the rig is connected to the cyclist’s geometry through the feature *Automatic Weights*, which assigns vertices of the mesh to the nearest bones based on spatial proximity. This initial weight assignment is further refined through manual weight painting, particularly in regions subject to complex deformations. In this manner, the influence of each rig bone on the cyclist’s body can be accurately controlled.

To ensure the correct positioning of the cyclist, the bicycle is added in the modeling scenario. The bicycle’s geometry was modeled using the CAD software Ansys[®] SpaceClaim[®] 2024 R1 and is based on a typical design of modern time-trial bikes used in official competitions. The following step of the procedure is the positioning of the cyclist in a riding pose, considering a stationary condition, with the pedaling motion not simulated. This approach simplifies the analysis while maintaining a realistic representation of the cycling posture. The cyclist is positioned on the bicycle from the standing to the riding pose through Blender rigging features, following the steps illustrated in Figure 3.

The final position is achieved by defining and optimizing multiple key angles crucial to the cycling posture. With reference to Table 1 and Figure 4, several angles are defined based on studies from the literature [6,52]: the sagittal torso angle (1), shoulder angle (2), elbow angle (3), forearm angle (4), right and left hip angle (5,6), right and left knee angle (7,8), right and left ankle angle (9,10). Following the positioning process, both the bicycle and cyclist geometries were exported and then smoothed and defeatured to enable efficient meshing for CFD simulations.

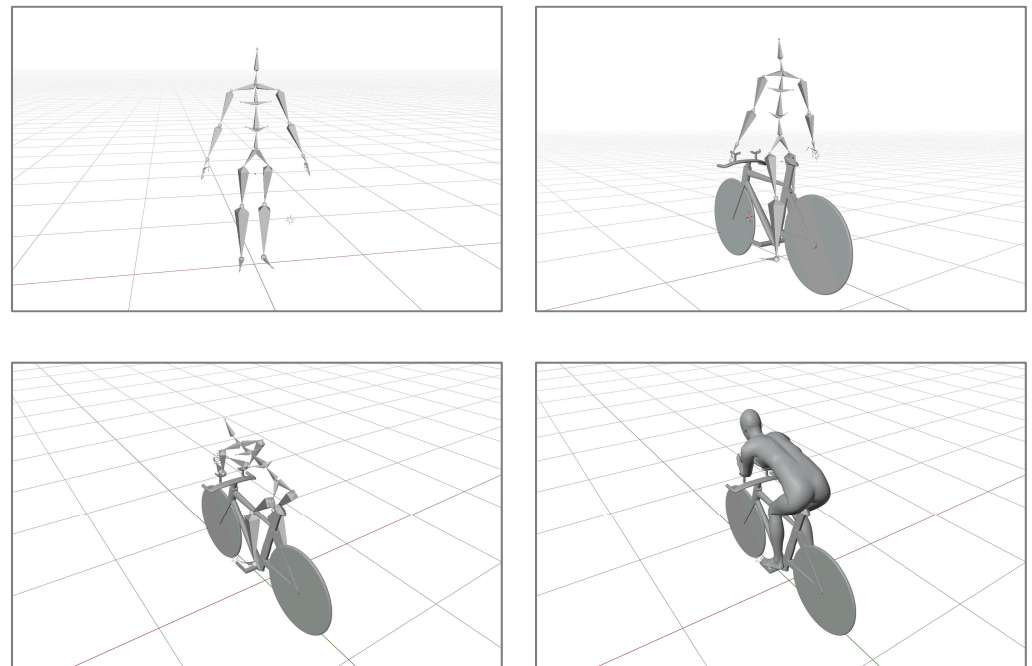


Figure 3. Cyclist’s positioning on the bicycle through the support articulation geometry.

Table 1. Cyclist posture angle values.

N°	Posture Angle	Value [deg]
1	Sagittal Torso Angle	18.6
2	Shoulder Angle	87.7
3	Elbow Angle	117.8
4	Forearm Angle	6.9
5	Right Hip Angle	76.0
6	Left Hip Angle	61.0
7	Right Knee Angle	56.9
8	Left Knee Angle	57.1
9	Right Ankle Angle	90.2
10	Left Ankle Angle	97.1

The helmet was reconstructed in 3D, based on actual time-trial products. Safety requirements regarding helmet thickness were considered in both the geometry design and the selection of shape parameters for optimization. It is important to highlight that both the bicycle and the helmet are generic models, and their specific characteristics do not influence the methodology illustrated or its implementation. In this case, the helmet’s maximum dimensions are 430 mm in length, 190 mm in width, and 220 mm in height. Figure 5 shows both the side and rear views of the helmet. The entire configuration, including the cyclist, bicycle, and helmet, occupies a frontal projected area of 0.7036 m². The described approach for cyclist modeling allows for easily modifying the cyclist’s position and replacing different types of bicycles or helmets. For instance, while the current case study focuses on an individual time-trial bicycle, it can be adapted to a standard road racing bicycle for other types of competitions. This facilitates simulations of various racing conditions compared to traditional approaches that rely on modeling the geometry by scanning actual cyclists, bicycles, and helmets [5,6,43,53].

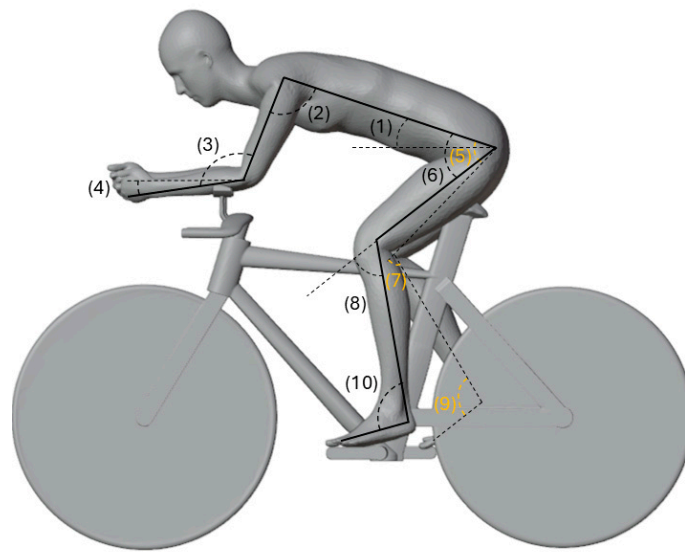


Figure 4. Cyclist posture angles definition.

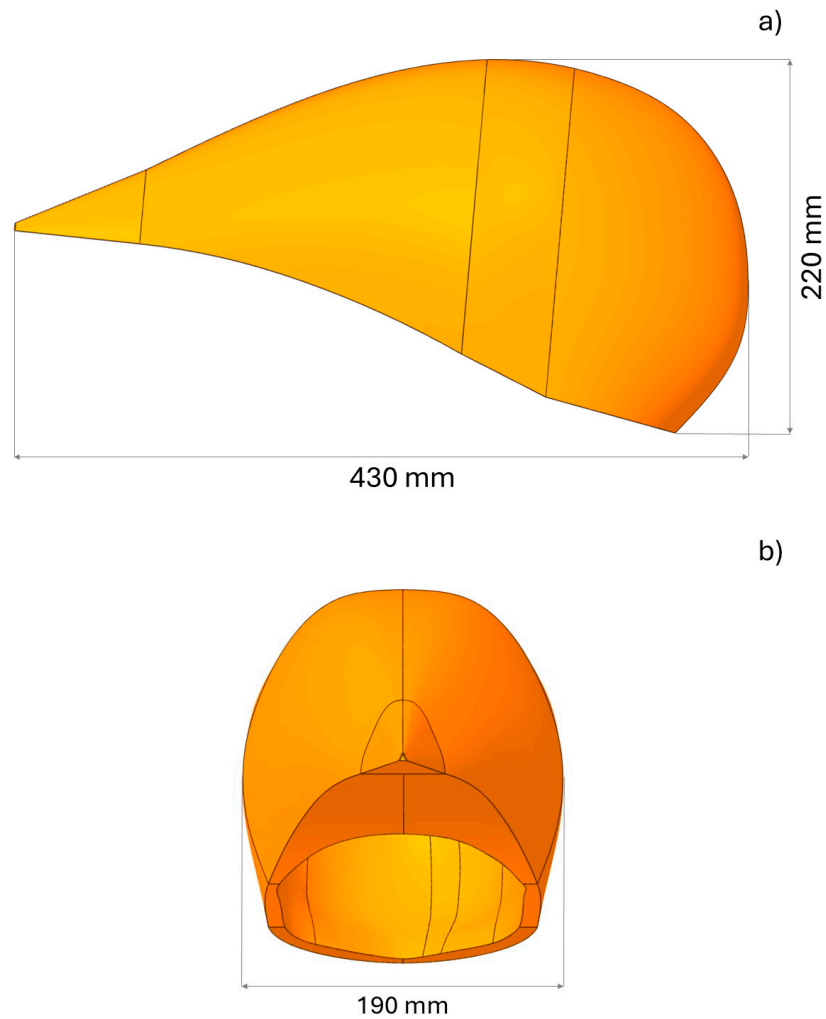


Figure 5. Helmet baseline geometry and maximum dimensions from the lateral (a) and back view (b).

3.2. Baseline and Morphed Configurations Analysis

The implementation of the cyclist CFD aerodynamic analysis was conducted using the commercial CFD solver Ansys[®] Fluent[®] 2024 R1. A baseline simulation was performed

to evaluate the aerodynamic properties of the entire assembly, in particular the drag force and drag coefficient, with a specific focus on the initial helmet geometry. Next, a design of experiments approach for optimization was implemented by defining the shape parameters used to modify the helmet through mesh morphing. In the final phase, the optimum drag force was evaluated through response surface optimization, and a reduced-order model was created for real-time visualization of the field variables. The simulations were performed on a workstation with an Intel® Xeon® W-2255 CPU running at 3.70 GHz with 32 GB of RAM, utilizing eight cores for the simulations.

3.2.1. Computational Domain Setup and Meshing

In the CFD analysis for external aerodynamics, it is essential to model not only the object of interest but also the surrounding computational domain, which represents the volume where the fluid flow interacts and evolves. This approach is critical for accurately capturing the flow characteristics and interactions between the object and the fluid. The computational domain must be sufficiently large to capture the flow dynamics accurately. Additionally, appropriate boundary conditions must be set to represent the influence of the fluid behavior around the body.

In this study, a steady RANS analysis is conducted using the K- ϵ standard turbulence model with enhanced near-wall treatment. A box-shape computational domain with a length of 10 m, a width of 3.5 m, and a height of 3 m was created, as visible in Figure 6. The front face of the domain serves as the inlet, while the back face is the outlet, as highlighted by the arrows. The foremost part of the bicycle is positioned 3.2 m from the inlet and in the middle relative to the width of the domain. A symmetry-type boundary condition is applied to the upper and lateral faces of the computational domain to simulate an open-air environment. This simplified representation effectively replicates far-field conditions in an open space rather than the enclosed nature of a wind tunnel. The approach ensures that edge effects are excluded from the analysis. These symmetry conditions are conceptually similar to applying a slip condition on a wall, where no friction is considered, and the flow conditions inside and outside the domain are treated equivalently.

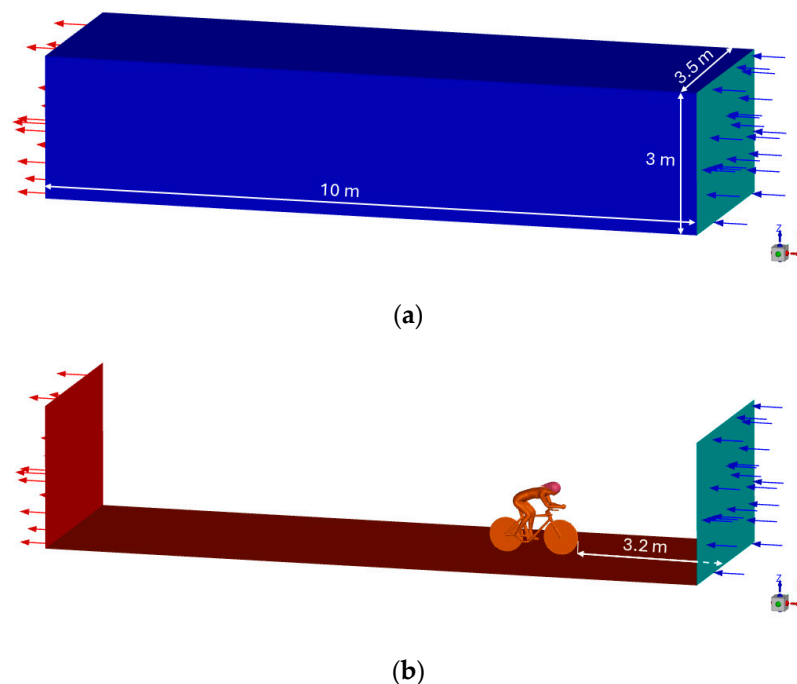


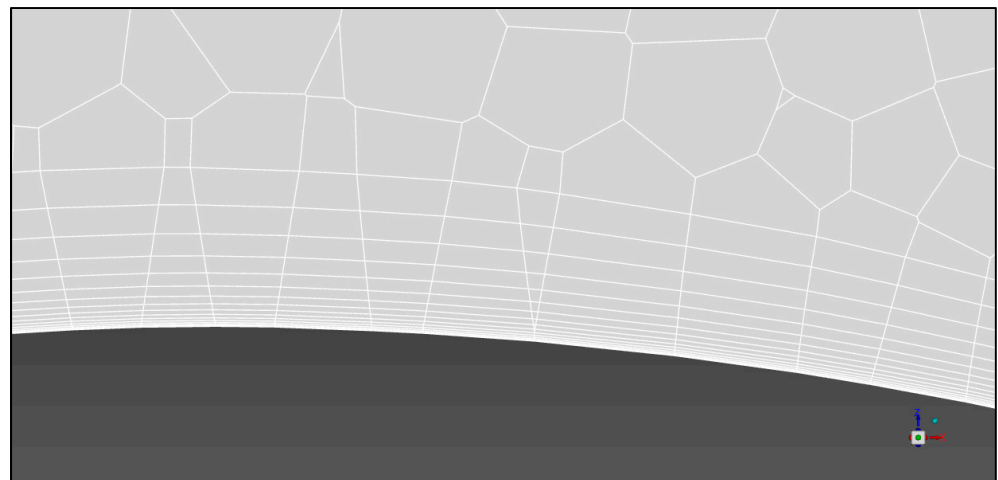
Figure 6. Computational domain shape (a) and cyclist's position inside the domain (b).

The computational domain was discretized using a poly-hexacore mesh, consisting of 4,083,840 cells, 20,521,854 faces, and 13,419,531 nodes. The external surfaces of the cyclist,

helmet, and bicycle were meshed with 173,517 faces, using a surface grid size ranging from 3 mm to 10 mm. The boundary layer mesh, illustrated in Figure 7, was modeled with 16 prism layers, maintaining an average $y^+ \approx 1.25$, as per similar literature studies [43,54]. The prism layer growing ratio was set to 1.3, with an initial wall-adjacent cell distance $y_p = 0.025$ mm, and transitioning to a maximum cell size of 80 mm in the coarser regions of the mesh.



(a)



(b)

Figure 7. Boundary layer mesh (a) and detailed view (b) around the helmet area.

3.2.2. Baseline Solution

The baseline solution was calculated using the helmet's initial design without applying mesh morphing. A uniform velocity of 15 m/s (54 km/h) is imposed at the inlet, while a relative pressure of 0 Pa is maintained at the outlet. To initialize the case, hybrid initialization was implemented, and the flow solution converged with approximately 1000 iterations. The computational setup involved using eight cores with a double precision solver on an Intel® Xeon® W-2255 CPU running at 3.70 GHz, with 32 GB of RAM. With these settings, a computational time of approximately 70 min is required for the baseline solution.

3.2.3. Mesh Morphing Setup and Morphed Configurations Solution

Mesh morphing was implemented by using the Ansys® RBF Morph™ Fluids 2024 R1 add-on in Fluent, focusing on modifying the helmet's front and back areas. In particular,

four shape modification parameters were defined, as illustrated in Table 2 and Figure 8. The parameter *front x* varies the depth of the frontal helmet along the *x* axis by moving it forward, while the other three parameters *scale x*, *scale y*, and *scale z* scale the back area of the helmet along the three coordinates *x*, *y*, and *z*. The morphing parameters were set using the *Encaps* feature in RBF Morph, which enables the deformation of a selected volume surrounding the geometry of interest. The transformation is then carried out through a combination of translation and scaling operations for the corresponding morphing parameters. The RBF mesh morphing approach ensures the preservation of mesh quality and topology, enabling the construction of reduced-order models (ROMs) for real-time visualization, as highlighted in previous studies [55–57]. This methodology can be implemented using independent codes by applying the mathematical principles behind RBF mesh morphing described in [29], providing a robust and adaptable framework for simulations in various applications.

Table 2. Morphing parameters' minimum and maximum values (refers to meshes in Figure 8).

Morphing Parameter	Minimum Value (Blue)	Maximum Value (Red)
<i>front x</i>	0	8
<i>scale x</i>	−8	4
<i>scale y</i>	−1	5
<i>scale z</i>	0	10

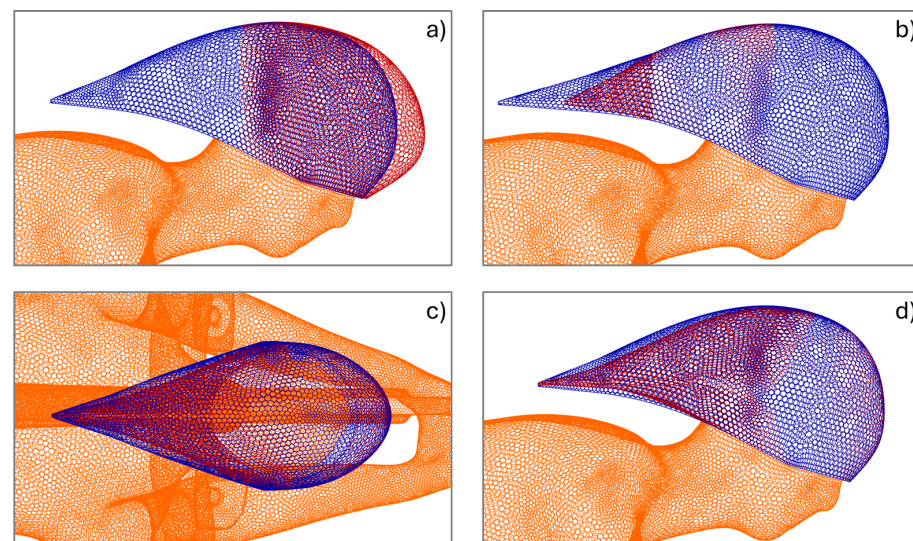


Figure 8. Helmet morphing parameters: front *x* (a), scale *x* (b), scale *y* (c), and scale *z* (d).

To generate a simulation dataset by varying the morphing parameters in the specified range, a DoE with 100 design configurations was implemented. The Latin hypercube sampling (LHS) technique was used to sample the design space optimally. Only morphing parameters were varied among these configurations, while the inlet velocity and other settings were maintained as in the baseline solution. Starting from the baseline converged data, approximately 100 additional iterations are required to converge a new morphed configuration, taking approximately 16 min to simulate each new case. Specifically, 8 min is required for mesh morphing, while 8 min is required for the CFD solution and output export. This results in a total time of 1670 min (almost 28 h, including the baseline solution), which must be taken into account when considering the two purposes of the full simulation: identifying a candidate point through response surface optimization and creating a reduced-order model for real-time visualization.

3.3. Response Surface Optimization Setup

Response surface methodology (RSM) was implemented to establish a correlation between the input and output parameters. In particular, the previously defined morphing parameters (*front x*, *scale x*, *scale y*, and *scale z*) were used as input parameters, while the drag force acting on the helmet, as well as the overall drag force acting on the helmet, cyclist, and bicycle, were selected as output parameters. The GARS method was selected to efficiently model and optimize the relationship between these variables. The final response surface model obtained from GARS allows for the identification of optimal morphing parameter settings that minimize drag, thus potentially improving aerodynamic performance. The predicted data, derived from the response surface, were compared with the observed data from full-order model simulations to evaluate the accuracy of the GARS model. This comparison, as illustrated in Figure 9, highlights the model’s ability to approximate the aerodynamic behavior with high accuracy.

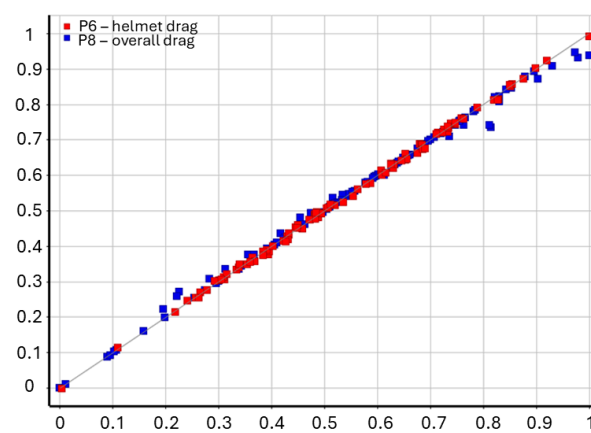


Figure 9. Predicted vs. observed normalized drag values.

The sensitivity analysis, as illustrated in Figure 10, provides insights into the impact of normalized morphing parameters on the drag forces. Local sensitivity curves describe how variations in the parameters influence drag. For example, the curve for *scale x* (red) consistently shows a downward trend, suggesting that increasing *scale x* reduces the drag force. Conversely, the curves for *front x* (blue), *scale y* (green), and *scale z* (yellow) exhibit non-linear behaviors, indicating complex interactions with the drag force that can both increase and decrease drag depending on the parameter levels.

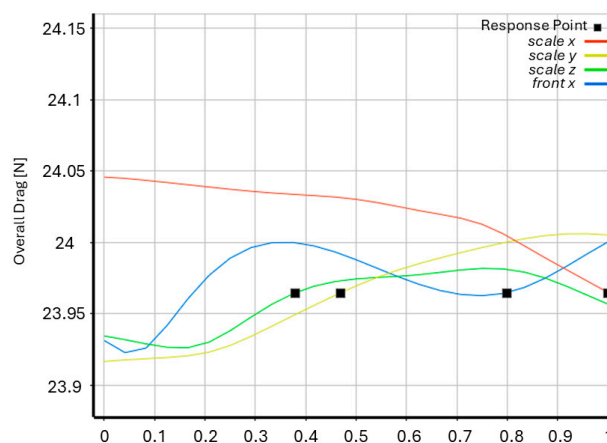


Figure 10. Local sensitivity curves for overall drag optimization.

3.4. Reduced-Order Model Implementation

The reduced-order model (ROM) was implemented to enhance the real-time visualization of critical aerodynamic variables, such as pressure distribution, wall shear stress, and turbulence intensity. The ROM was created using the POD method within Ansys® Twin Builder, based on 50 snapshots from full-order CFD simulations, and validated with an additional set of 50 snapshots.

This approach significantly reduces computational time while maintaining a sufficiently high accuracy. A full-order simulation, including mesh morphing and aerodynamic analysis for a single configuration, requires approximately 16 min. In contrast, the ROM can generate results in real time, using 10 selected modes, with a maximum error in the pressure of approximately 2.5%, corresponding to 1.8 Pa, compared with the full-order model. The decision to select 10 modes instead of the 15 suggested by the software algorithm was implemented to reduce the ROM's computational footprint, facilitating its integration into virtual and augmented reality applications in mobile devices. Although this reduction increases the maximum ROM error for pressure from 1% to 2.5%, this was considered acceptable, given the trade-offs in portability and real-time performance. Table 3 presents the ROM error evaluation for the first 10 design points in the DoE, where 5 of these were included in ROM generation, and the remaining 5 were left out for ROM validation.

Table 3. ROM error evaluation for the first 10 design points.

DP	Front X	Scale X	Scale Y	Scale Z	Selected	ROM Error (%)
1	0	0	0	0	YES	0.313
2	4	−8	−1	5	YES	0.225
3	8	4	5	10	YES	0.285
4	0.522	3.58	1.90	3.49	NO	1.740
5	7.78	3.15	2.67	9.93	NO	1.064
6	0.037	1.32	3.56	2.53	YES	0.319
7	1.95	−5.99	−0.637	8.86	NO	2.131
8	2.28	0.704	4.71	6.56	NO	2.215
9	6.38	1.87	2.14	3.12	YES	0.332
10	4.58	−5.80	3.62	5.61	NO	1.363

By integrating ROM into the design workflow, significant computational savings are achieved without compromising the accuracy of aerodynamic predictions. This enables the design team to efficiently explore and refine various helmet geometries, with subsequent validations to be performed on a few selected designs. Additionally, the reduction in computational demands supports broader design space exploration, including potential future extensions to more complex configurations, such as the inclusion of the cyclist position and bicycle geometry, facilitating comprehensive aerodynamic analyses.

4. Results

4.1. Response Surface Optimization

The application of response surface optimization (RSO) led to the minimization of drag force at a designated candidate point. To better understand the influence of each parameter on the drag force, a series of response surfaces were plotted, as shown in Figure 11. These surfaces were analyzed to observe the behavior of the drag force with individual parameters, facilitating a detailed analysis of their respective effects.

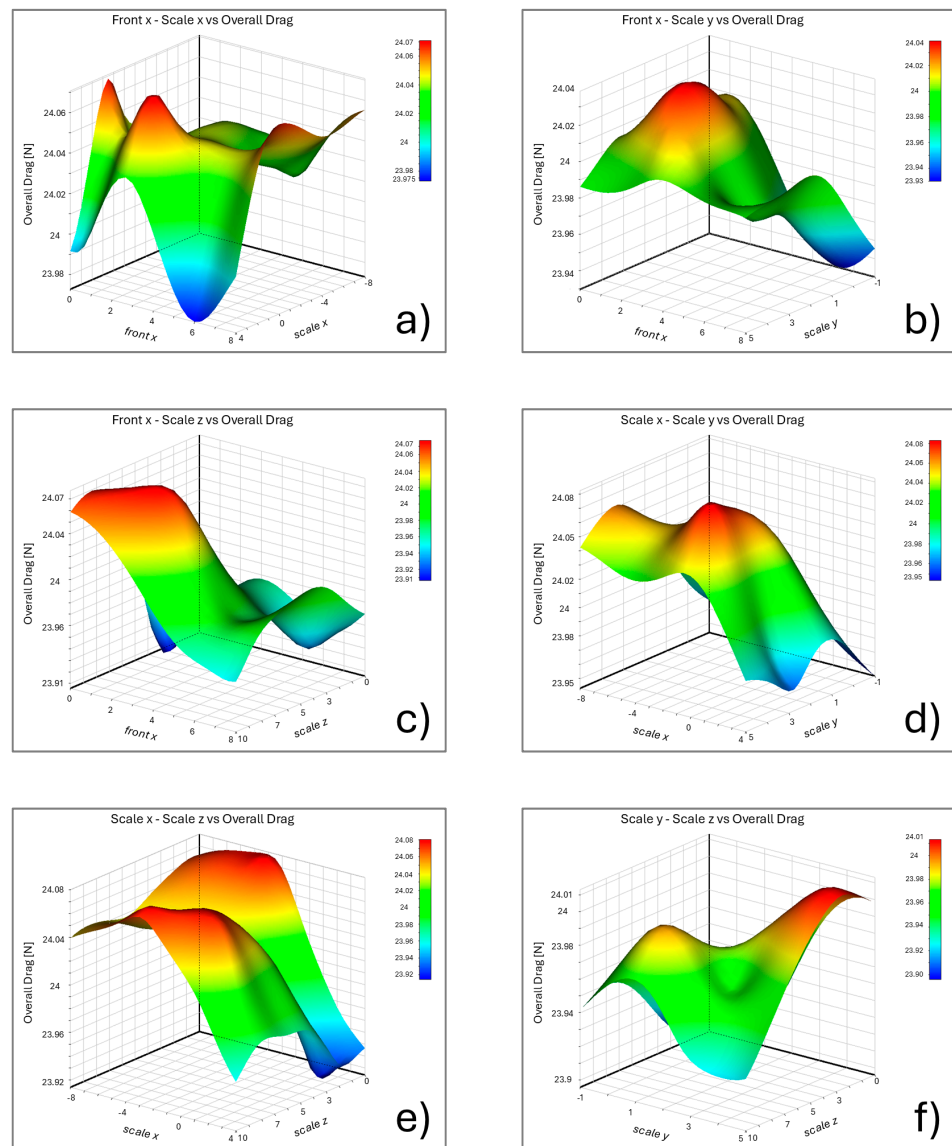


Figure 11. Response surfaces for overall drag vs. morphing parameters.

Given that the optimization involved four parameters (*front x*, *scale x*, *scale y*, and *scale z*), six response surfaces in a three-dimensional space were plotted to capture the relationships between each pair of parameters (Figure 11a–f). This systematic approach allowed for a clear visualization of how changes in one parameter influence drag in conjunction with others. The use of response surfaces provided valuable insights into parameter sensitivities and interactions, leading to a final optimization characterized by the respective values of 6.40, 3.99, 1.85, and 3.89 for the parameters *front x*, *scale x*, *scale y*, and *scale z*, respectively. The optimization of the helmet’s shape yielded a 10.22% reduction in the drag force acting on the helmet and a 0.25% reduction in the total drag force.

4.2. Reduced-Order Model

RSO focused on optimizing an individual parameter, specifically the overall drag force on the cyclist. However, the use of a ROM offers a more comprehensive understanding of the system’s aerodynamics. Figures 12–14 highlight how the cyclist’s ROM facilitates real-time visualization of three field quantities—static pressure, turbulence intensity, and wall shear stress—for baseline and optimized helmet configurations. Once the ROM is loaded within a visualization tool, the input parameters are associated with adjustable

sliders, which allow changing each input parameter within its validity range. Each action on the sliders is followed by a refresh of the visualization, consisting of a shape change (based on the ROM of the mesh) and of the displayed output color map (based on the ROM of the current output). Such refresh occurs almost in real time, allowing a quick inspection of the effect of combined input parameters.

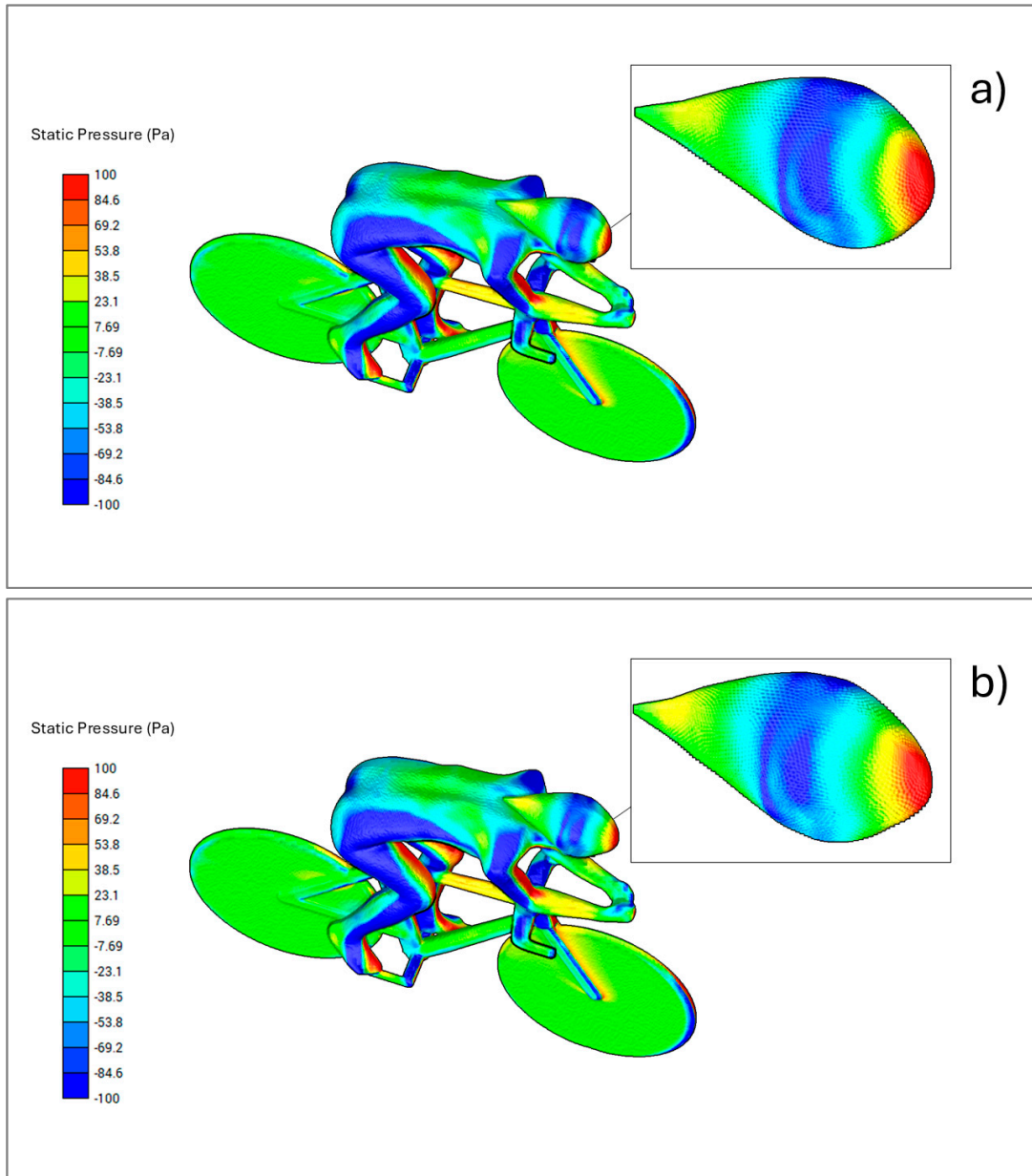


Figure 12. Real-time pressure evaluation of the baseline (a) and optimized (b) helmet.

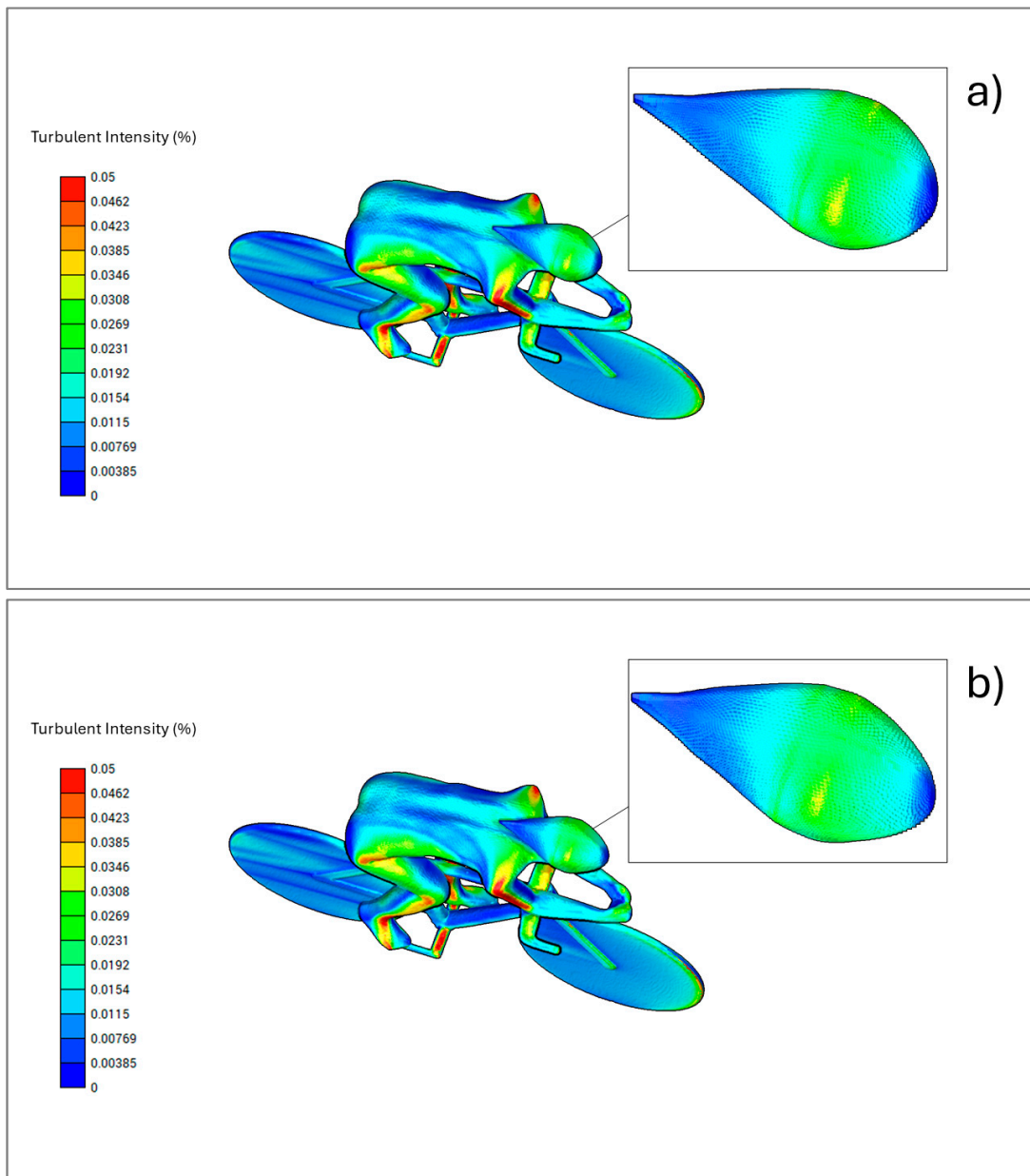


Figure 13. Real-time turbulence intensity evaluation of the baseline (a) and optimized (b) helmet.

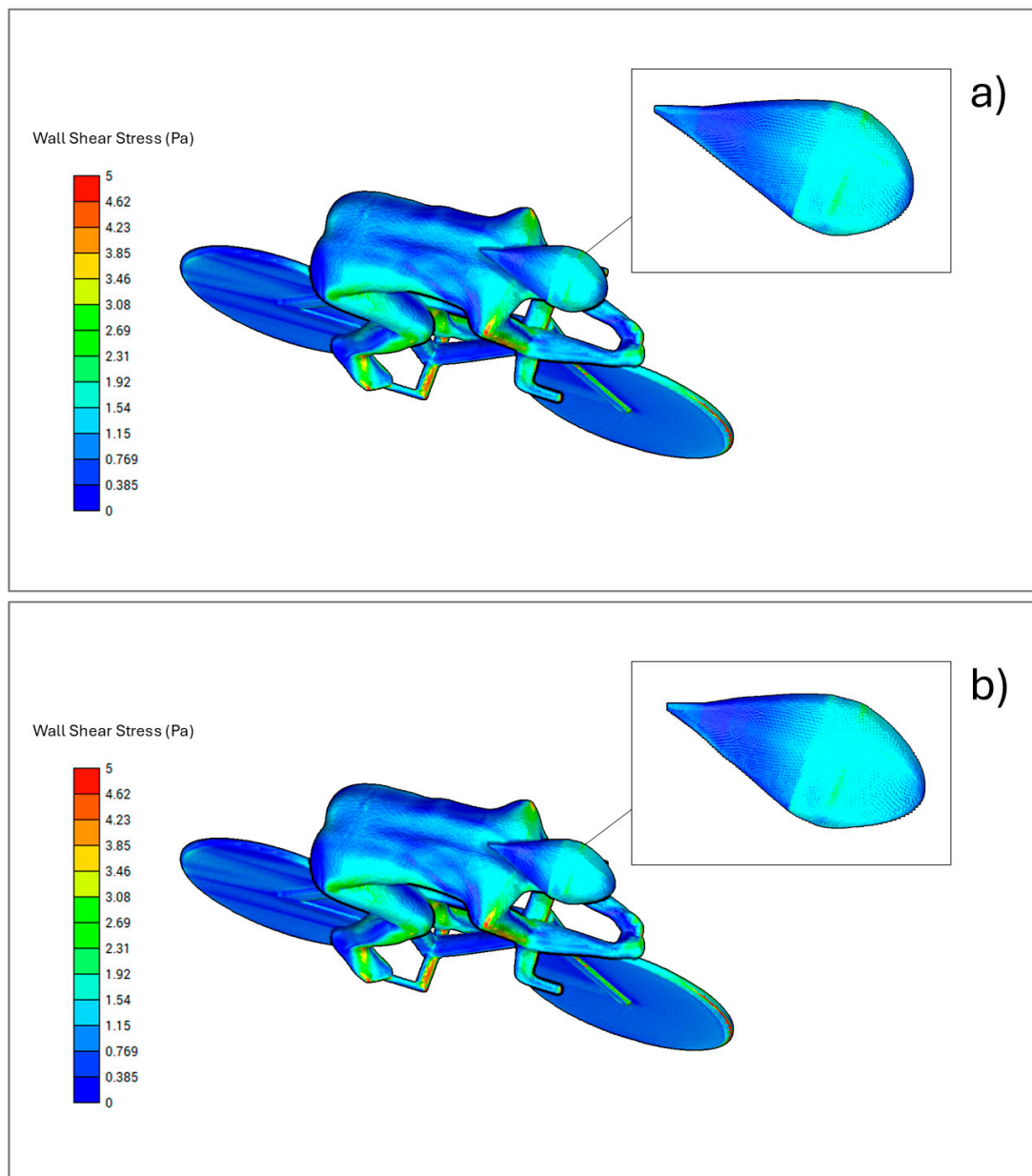


Figure 14. Real-time wall shear stress evaluation of the baseline (a) and optimized (b) helmet.

By analyzing these fields, the cyclist's aerodynamics can be better understood, providing clear guidance on how to optimize performance. Notably, the results show that turbulence intensity and wall shear stress in particular (as visible in Figures 13 and 14) vary not only on the helmet but also on the cyclist's back and legs, where significant aerodynamic interactions occur, with lower values being observed when the optimized helmet shape is investigated. As observed in previous draft cycling studies [53], reducing both the overpressure on the cyclist's front and the lower pressure on the back plays a crucial role in minimizing drag.

5. Conclusions

In this study, a comprehensive methodology was developed and implemented for optimizing the aerodynamics of a cyclist's helmet for time-trial competitions, leveraging advanced techniques, such as response surface methodology (RSM) and reduced-order

models (ROMs). The approach focused on improving helmet design to reduce aerodynamic drag for enhancing performance during time-trial events.

The first step of the process involved the implementation of the cyclist, helmet, and bicycle geometries, with careful attention to the cyclist's posture and positioning to simulate typical individual time-trial conditions. Mesh morphing techniques were applied to enable flexible, parametric modification of the helmet's geometry, optimizing it for aerodynamic performance while maintaining adherence to safety standards. Through the DoE and RSM, the impact of individual shape parameters on aerodynamic drag was explored. This facilitated the identification of optimal configurations, where significant drag reductions were achieved both for the helmet itself and for the overall cyclist–helmet system. The RSM provided valuable insights into the relationship between helmet geometry and aerodynamic resistance, allowing for a systematic approach to design refinement. The use of ROMs further enhanced the optimization process by providing real-time assessments of aerodynamic variables, such as pressure distribution, wall shear stress, and turbulence intensity. The ROM enabled a rapid evaluation of the design modifications, significantly reducing computational costs and improving the feasibility of real-time design iteration. Notably, the analysis highlighted that aerodynamic effects, particularly turbulence intensity and wall shear stress, do not only concentrate on the helmet but also influence the cyclist's back and legs. This underscores the importance of considering the interaction between the helmet and the entire body of the cyclist when optimizing for drag reduction.

A range of opportunities for future research and development present themselves upon the foundation laid by this study. The implementation of three-dimensional aerodynamic fields, such as velocity, in the ROM would allow for a more detailed investigation of the effects of different cyclist postures and bicycle geometries, combining geometry modifications with morphing techniques to refine overall aerodynamics. Additional attention could be given to exploring further shape parameters, particularly on the front and side areas of the helmet, as well as the cyclist's bicycle, to enhance performance even more. Another critical step would involve verifying the simulation results through experimental data obtained from pressure sensors placed on the cyclist's body and the bicycle. Integrating these sensor data into the ROM would likely increase the accuracy of the simulations, offering a more personalized optimization. Moreover, customization of the helmet interior, using a 3D scan of the cyclist's head, could provide a perfect fit, thereby improving both comfort and safety. Finally, integrating the aerodynamic model into virtual and augmented reality platforms would enable enhanced visualization of aerodynamic fields and real-time analysis on wearable devices.

Author Contributions: Methodology, M.E.B.; Software, A.L., C.G. and M.E.B.; Investigation, E.D.M.; Data curation, A.L.; Writing—original draft, E.D.M.; Writing—review & editing, P.P.V.; Supervision, C.G., M.E.B. and P.P.V.; Funding acquisition, P.P.V. All authors have read and agreed to the published version of the manuscript.

Funding: The research was funded by the Italian Ministry for University and Research within the National Center for HPC, Big Data and Quantum Computing, Project CN_0000013–CUP E83C22003230001, Mission 4 Component 2 Investment 1.4, funded by the European Union–NextGenerationEU.

Data Availability Statement: The original contributions presented in the study are included in the article, further inquiries can be directed to the corresponding author.

Conflicts of Interest: The authors declare no conflict of interest.

Abbreviations

CAD	Computer-Aided Design
CCD	Central Composite Design
CFD	Computational Fluid Dynamics
DNS	Direct Numerical Simulation
DoE	Design of Experiments

DoF	Degree of Freedom
FF	Full Factorial
GA	Genetic Aggregation
GARS	Genetic Aggregation Response Surface
ITT	Individual Time Trial
LES	Large Eddy Simulation
LHS	Latin Hypercube Sampling
L-S	Lyapunov–Schmidt
MOGA	Multi-Objective Genetic Algorithm
MOR	Model Order Reduction
PCA	Principal Component Analysis
POD	Principal Orthogonal Decomposition
RANS	Reynolds-Averaged Navier–Stokes
RBF	Radial Basis Function
ROM	Reduced-Order Model
RSM	Response Surface Methodology
RSO	Response Surface Optimization
SVD	Singular Value Decomposition

References

- Alam, F.; Chowdhury, H.; Moria, H. A review on aerodynamics and hydrodynamics in sports. *Energy Procedia* **2019**, *160*, 798–805. [[CrossRef](#)]
- Malizia, F.; Blocken, B. Cyclist aerodynamics through time: Better, faster, stronger. *J. Wind. Eng. Ind. Aerodyn.* **2021**, *214*, 104673. [[CrossRef](#)]
- Kyle, C.R.; Burke, E. Improving the racing bicycle. *Mech. Eng.* **1984**, *106*, 34–35.
- Grappe, F.; Candau, R.; Belli, A.; Rouillon, J. Aerodynamic drag in field cycling with special reference to the Obree’s position. *Ergonomics* **1997**, *40*, 1299–1311. [[CrossRef](#)]
- Malizia, F.; van Druenen, T.; Blocken, B. Impact of wheel rotation on the aerodynamic drag of a time trial cyclist. *Sports Eng.* **2021**, *24*, 3. [[CrossRef](#)]
- Van Druenen, T.; Blocken, B. Aerodynamic impact of cycling postures on drafting in single paceline configurations. *Comput. Fluids* **2023**, *257*, 105863. [[CrossRef](#)]
- Chowdhury, H.; Alam, F. An experimental study on aerodynamic performance of time trial bicycle helmets. *Sports Eng.* **2014**, *17*, 165–170. [[CrossRef](#)]
- Novak, J.; Burton, D.; Crouch, T. Aerodynamic test results of bicycle helmets in different configurations: Towards a responsive design. *Proc. Inst. Mech. Eng. Part P J. Sports Eng. Technol.* **2019**, *233*, 268–276. [[CrossRef](#)]
- Team Visma Lease a Bike. Team Visma | Lease a Bike Launches New Time Trial Helmet. 2024. Available online: www.teamvismaleaseabike.com/news/news/team-visma-lease-a-bike-launches-new-time-trial-helmet (accessed on 12 April 2024).
- Blocken, B.; Malizia, F.; van Druenen, T. CFD analysis of chest fairings in time trial cycling. *J. Wind. Eng. Ind. Aerodyn.* **2024**, *248*, 105709. [[CrossRef](#)]
- Rowley, C.W.; Dawson, S.T.M. Model Reduction for Flow Analysis and Control. *Annu. Rev. Fluids Mech.* **2017**, *49*, 387–417. [[CrossRef](#)]
- Benner, P.; Gugercin, S.; Willcox, K. A Survey of Projection-Based Model Reduction Methods for Parametric Dynamical Systems. *SIAM Rev.* **2015**, *57*, 483–531. [[CrossRef](#)]
- Taira, K.; Hemati, M.S.; Brunton, S.L.; Sun, Y.; Duraisamy, K.; Bagheria, S.; Dawson, S.T.M.; Yeh, C. Modal Analysis of Fluid Flows: Application and Outlook. *AIAA J.* **2020**, *58*, 998–1022. [[CrossRef](#)]
- Ripepi, M.; Verveld, M.J.; Karcher, N.W.; Franz, T.; Abu-Zurayk, M.; Görtz, S.; Kier, T.M. Reduced-order models for aerodynamic applications, loads and MDO. *CEAS Aeronaut. J.* **2018**, *9*, 171–193. [[CrossRef](#)]
- Li, K.; Kou, J.; Zhang, W. Unsteady aerodynamic reduced-order modeling based on machine learning across multiple airfoil. *Aerosp. Sci. Technol.* **2021**, *119*, 107173. [[CrossRef](#)]
- Liu, K.; Li, D.; Xiang, J. Reduced-order modeling of unsteady aerodynamics of a flapping wing based on the Volterra theory. *Results Phys.* **2017**, *7*, 2451–2457. [[CrossRef](#)]
- Sirovich, L. Turbulence and the Dynamics of Coherent Structures. Parts I–III. *Q. Appl. Math.* **1987**, *45*, 561–590. [[CrossRef](#)]
- Holmes, P.; Lumley, J.L.; Berkooz, G. *Turbulence, Coherent Structures, Dynamical Systems and Symmetry*; Cambridge Monographs on Mechanics; Cambridge University Press: Cambridge, UK, 1996. [[CrossRef](#)]
- Willcox, K.; Peraire, J. Balanced model reduction via the proper orthogonal decomposition. *AIAA J.* **2002**, *40*, 2323–2330. [[CrossRef](#)]
- Lassila, T.; Manzoni, A.; Quarteroni, A.; Rozza, G. Model Order Reduction in Fluid Dynamics: Challenges and Perspectives. In *Reduced Order Methods for Modeling and Computational Reduction*; Quarteroni, A., Rozza, G., Eds.; MS&A—Modeling, Simulation and Applications; Springer: Cham, Switzerland, 2014; Volume 9. [[CrossRef](#)]

21. Myers, R.H.; Montgomery, D.C.; Anderson-Cook, C.M. *Response Surface Methodology: Process and Product Optimization Using Designed Experiments*, 4th ed.; John Wiley & Sons: Hoboken, NJ, USA, 2016.
22. Box, G.E.P.; Draper, N.R. *Empirical Model-Building and Response Surfaces*; John Wiley & Sons: New York, NY, USA, 1987.
23. Biancolini, M.E.; Costa, E.; Cella, U.; Groth, C.; Veble, G.; Andrejašič, M. Glider fuselage-wing junction optimization using CFD and RBF mesh morphing. *Aircr. Eng. Aerosp. Technol.* **2016**, *88*, 740–752. [[CrossRef](#)]
24. Berkooz, G.; Holmes, P.J.; Lumley, J. The Proper Orthogonal Decomposition in the analysis of turbulent flows. *Annu. Rev. Fluid Mech.* **2003**, *25*, 539–575. [[CrossRef](#)]
25. Lu, K.; Zhang, K.; Zhang, H.; Gu, X.; Jin, Y.; Zhao, S.; Fu, C.; Yang, Y. A review of model order reduction methods for large-scale structure systems. *Shock. Vib.* **2021**, *2021*, 6631180. [[CrossRef](#)]
26. Geronzi, L.; Martinez, A.; Rochette, M.; Yan, K.; Bel-Brunon, A.; Haignon, P.; Escrig, P.; Tomasi, J.; Daniel, M.; Lalande, A.; et al. Computer-aided shape features extraction and regression models for predicting the ascending aortic aneurysm growth rate. *Comput. Biol. Med.* **2023**, *162*, 107052. [[CrossRef](#)]
27. Kerschen, G.; Golinval, J.C.; Vakasis, A.; Bergman, L. The Method of Proper Orthogonal Decomposition for Dynamical Characterization and Order Reduction of Mechanical Systems: An Overview. *Nonlinear Dyn.* **2005**, *41*, 147–169. [[CrossRef](#)]
28. De Boer, A.; Van der Schoot, M.S.; Bijl, H. Mesh deformation based on radial basis function interpolation. *Comput. Struct.* **2007**, *85*, 784–795. [[CrossRef](#)]
29. Biancolini, M.E. *Fast Radial Basis Functions for Engineering Applications*; Springer International Publishing: Cham, Switzerland, 2017. [[CrossRef](#)]
30. Biancolini, M.E.; Viola, I.M.; Riotte, M. Sails trim optimisation using CFD and RBF mesh morphing. *Comput. Fluids* **2014**, *93*, 46–60. [[CrossRef](#)]
31. Biancolini, M.E.; Bene, C.D.; Larsson, T.; Groth, C. Evaluation of go-kart aerodynamic efficiency using CFD, RBF mesh morphing and lap time simulation. *Int. J. Aerodyn.* **2016**, *5*, 146–171. [[CrossRef](#)]
32. Biancolini, M.E.; Valentini, P.P. Virtual human bone modelling by interactive sculpting, mesh morphing and force-feedback. *Int. J. Interact. Des. Manuf. (IJIDeM)* **2018**, *12*, 1223–1234. [[CrossRef](#)]
33. Kleijnen, J.P.C. An overview of the design and analysis of simulation experiments for sensitivity analysis. *Eur. J. Oper. Res.* **2005**, *164*, 287–300. [[CrossRef](#)]
34. Álvarez, M.J.; Ilzarbe, L.; Viles, E.; Tanco, M. The use of genetic algorithms in response surface methodology. *Qual. Technol. Quant. Manag.* **2009**, *6*, 295–307. [[CrossRef](#)]
35. Abunike, C.E.; Okoro, O.I.; Aphale, S.S. Intelligent optimization of switched reluctance motor using genetic aggregation response surface and multi-objective genetic algorithm for improved performance. *Energies* **2022**, *15*, 6086. [[CrossRef](#)]
36. Montgomery, D.C.; Peck, E.A.; Vining, G.G. *Introduction to Linear Regression Analysis*, 6th ed.; John Wiley & Sons: Hoboken, NJ, USA, 2021.
37. Boer, E.P.; de Beurs, K.M.; Hartkamp, A.D. Kriging and thin plate splines for mapping climate variables. *Int. J. Appl. Earth Obs. Geoinf.* **2001**, *3*, 146–154. [[CrossRef](#)]
38. Wu, H.; Zhang, J.T. *Nonparametric Regression Methods for Longitudinal Data Analysis: Mixed-Effects Modeling Approaches*; John Wiley & Sons: New York, NY, USA, 2006. [[CrossRef](#)]
39. Constantine, P.G.; Eldred, M.S.; Phipps, E.T. Sparse Pseudospectral Approximation Method. *Comput. Methods Appl. Mech. Eng.* **2012**, *229–232*, 1–12. [[CrossRef](#)]
40. Versteeg, H.K.; Malalasekera, W. *An Introduction to Computational Fluid Dynamics—The Finite Volume Method*, 2nd ed.; Pearson Education: Harlow, UK, 2006.
41. Corson, D.; Jaiman, R.; Shakib, F. Industrial application of RANS modelling: Capabilities and needs. *Int. J. Comput. Fluid Dyn.* **2009**, *23*, 337–347. [[CrossRef](#)]
42. Che Sidik, N.A.; Yusof, S.N.A.; Asako, Y.; Mohamed, S.B.; Aziz, A. A Short Review on RANS Turbulence Models. *CFD Lett.* **2020**, *12*, 83–96. [[CrossRef](#)]
43. Van Druenen, T.; Blocken, B. CFD simulations of cyclist aerodynamics: Impact of computational parameters. *J. Wind. Eng. Ind. Aerodyn.* **2024**, *249*, 105714. [[CrossRef](#)]
44. Brown, C.; Burton, D.; Crouch, T.; Thompson, M.C. The influence of turbulence on cycling aerodynamics. *J. Wind. Eng. Ind. Aerodyn.* **2023**, *242*, 105575. [[CrossRef](#)]
45. DINED Anthropometric Database | Mannequin. 2020. Available online: <https://dined.io.tudelft.nl/en/mannequin/introduction> (accessed on 12 October 2023).
46. Robinette, K.M.; Daanen, H.; Paquet, E. The CAESAR project: A 3-D surface anthropometry survey. In Proceedings of the 2nd International Conference on 3-D Digital Imaging and Modeling (3DIM'99), Ottawa, ON, Canada, 4–8 October 1999; IEEE Computer Society: Washington, DC, USA, 1999; pp. 380–386.
47. CAESAR. Civilian American and European Surface Anthropometry Resource Project. Available online: <https://www.sae.org/standardsdev/tsb/cooperative/caesar.htm> (accessed on 12 October 2023).
48. Blender Foundation—Blender 2.79 Manual: Rigging. Available online: <https://docs.blender.org/manual/en/2.79/rigging/index.html> (accessed on 9 December 2024).
49. Xu, Z.; Zhou, Y.; Kalogerakis, E.; Landreth, C.; Singh, K. RigNet: Neural Rigging for Articulated Characters. *ACM Trans. Graph.* **2020**, *39*, 58:1–58:14. [[CrossRef](#)]

50. De la Torre, R.; Oña, E.D.; Victores, J.G.; Jardón Huete, A. SpasticSim: A synthetic data generation method for upper limb spasticity modelling in neurorehabilitation. *Sci. Rep.* **2024**, *14*, 1646. [[CrossRef](#)]
51. DeVries, R.P.; Sereno, P.C.; Vidal, D.; Baumgart, S.L. Reproducible Digital Restoration of Fossils Using Blender. *Front. Earth Sci.* **2022**, *10*, 833379. [[CrossRef](#)]
52. Blocken, B.; Toparlar, Y.; van Druenen, T.; Andrienne, T. Aerodynamic drag in cycling team time trials. *J. Wind Eng. Ind. Aerodyn.* **2018**, *182*, 128–145. [[CrossRef](#)]
53. Blocken, B.; Defraeye, T.; Koninckx, E.; Carmeliet, J.; Hespel, P. CFD simulations of the aerodynamic drag of two drafting cyclists. *Comput. Fluids* **2013**, *71*, 435–445. [[CrossRef](#)]
54. Blocken, B.; Toparlar, Y.; Andrienne, T. Aerodynamic benefit for a cyclist by a following motorcycle. *J. Wind. Eng. Ind. Aerodyn.* **2016**, *155*, 1–10. [[CrossRef](#)]
55. Biancolini, M.E.; Capellini, K.; Costa, E.; Groth, C.; Celi, S. Fast interactive CFD evaluation of hemodynamics assisted by RBF mesh morphing and reduced order models: The case of aTAA modelling. *Int. J. Interact. Des. Manuf. (IJIDeM)* **2020**, *14*, 1227–1238. [[CrossRef](#)]
56. Kardampiki, E.; Vignali, E.; Haxhiademi, D.; Federici, D.; Ferrante, E.; Porziani, S.; Chiappa, A.; Groth, C.; Cioffi, M.; Biancolini, M.E.; et al. The hemodynamic effect of modified blalock–taussig shunt morphologies: A computational analysis based on reduced order modeling. *Electronics* **2022**, *11*, 1930. [[CrossRef](#)]
57. Geronzi, L.; Fanni, B.M.; De Jong, B.; Roest, G.; Kenjeres, S.; Celi, S.; Biancolini, M.E. A Parametric 3D Model of Human Airways for Particle Drug Delivery and Deposition. *Fluids* **2024**, *9*, 27. [[CrossRef](#)]

Disclaimer/Publisher’s Note: The statements, opinions and data contained in all publications are solely those of the individual author(s) and contributor(s) and not of MDPI and/or the editor(s). MDPI and/or the editor(s) disclaim responsibility for any injury to people or property resulting from any ideas, methods, instructions or products referred to in the content.